



OPEN

Pathogenesis of impaired glucose tolerance in rats based on transcriptome analysis

Ran Yi^{1,2,5}, Yu Xie^{3,4,5}, Yue Fan^{1,2}, Xinyi Liu^{1,2}, Zixuan Yang^{1,2} & Shangjian Liu²✉

Impaired glucose tolerance (IGT) is a transitional stage in the development of Type 2 diabetes mellitus (T2DM), but understanding its pathogenesis is currently insufficient. This study established the IGT rats through a high-fat diet combined with intraperitoneal Streptozotocin (STZ) injection to investigate the pathogenesis via transcriptomic profiling of liver tissues. Through transcriptome analysis, a total of 860 up-regulated and 707 down-regulated differentially expressed genes (DEGs) were identified. Enrichment analysis highlighted the PPAR signaling pathway as central to the pathology of IGT. Protein-protein interaction (PPI) network analysis identified IL-1 β , Stat1, Igf-1, and Cyp7a1 as Target DEGs (T-DEGs), which were validated by Western blot analysis. Elevated serum levels of IL-6, IFN γ , TNF α , and IL-1 β were confirmed via ELISA analysis. The results suggested that signaling pathways such as STAT1/PPAR γ /IGF-1, STAT1/PPAR γ /Cyp7a1, and STAT1/PPAR γ /IL-1 β may play crucial roles in the pathogenesis of IGT. These findings provide insight into potential mechanisms and targets for early diagnosis and therapeutic intervention.

Keywords Impaired glucose tolerance (IGT), Bioinformatics analysis, Transcriptome, Differentially expressed genes (DEGs), PPAR signaling pathway.

Impaired glucose tolerance (IGT) is an early stage of type 2 diabetes mellitus (T2DM) without typical clinical symptoms. Relevant data estimate that more than 1.31 billion people are expected to suffer from T2DM by 2050¹, and the global prevalence of IGT is projected to increase to 10%, or 638 million people, by 2045². These figures indicate an alarming increase in the prevalence of T2DM and IGT worldwide. As a reserve force of T2DM, IGT has a conversion rate of up to 50% within 5 years, marking an increased risk of T2DM and cardiovascular-related diseases³. Once individuals enter the IGT stage, their health risk increases significantly. However, the IGT population has a low awareness rate and an insidious onset, which seriously affects life quality. Scholars have found that Homeostatic Model Assessment of Insulin Resistance (HOMA-IR) levels are already elevated in IGT and can be regarded as an independent risk factor for progression from IGT to T2DM⁴. Hyperglycemia during the IGT stage also increases levels of related inflammatory cytokines, which are risk factors for microvascular or macrovascular disease⁵. Moreover, disorders in both glucose and lipid metabolism during the IGT stage may contribute to end-organ damage, such as kidney disease, heart disease, and retinopathy⁶.

As a critical period in the conversion to T2DM, IGT exhibits a high degree of reversibility, and the likelihood of blood glucose normalization in IGT patients can be increased through medication and lifestyle intervention⁷. Early screening and treatment of the IGT population can not only advance the timing of diabetes treatment, improve the reversal rate of prediabetes, and reduce the number of people progressing to diabetes, but also control the occurrence and development of diabetes and prevent cardiovascular and other related complications. As research on disease occurrence mechanisms advances, some studies have identified risk factors associated with IGT. Under the influence of inflammatory cytokines, alteration in the insulin IRS/PI3-K signaling pathway may be associated with the incidence of prediabetes⁸. Transcriptomics plays a crucial role in elucidating disease mechanisms by conducting unbiased comparisons of transcriptomic profiles between healthy and diseased tissues, characterizing disease-associated genetic alterations, and identifying biological pathways⁹. With the continuous advancement of transcriptomic sequencing technology, the core genes and associated pathways of diabetes and related complications, such as diabetic nephropathy and diabetic retinopathy have been identified^{10,11}. However, the pathogenesis of IGT has not yet been elucidated, and the intrinsic transcriptomic mechanisms underlying changes in glucose metabolism during the IGT period remain unclear. Transcriptomics

¹Beijing University of Chinese Medicine, Beijing, China. ²Dongzhimen Hospital, Beijing University of Chinese Medicine, Beijing, China. ³Chinese Medicine Department, The First People Hospital of Yunnan Province, Kunming, Yunnan, China. ⁴The Affiliated Hospital of Kunming University of Science and Technology, Kunming, Yunnan, China.

⁵Ran Yi and Yu Xie contributed equally to this work. ✉email: dzmyylsj@163.com

is a valuable tool for investigating the mechanisms of IGT development and facilitating the diagnosis, treatment, and prevention of this disease. The liver, as the central organ regulating glucose homeostasis, plays a critical role in glycogen breakdown and storage, and serves as a major site of insulin resistance (IR)¹². To investigate the molecular mechanisms underlying impaired IGT, transcriptome sequencing analysis was performed on liver tissues from the IGT and Control (Ctrl) groups to identify altered expressed genes, core genes, and potential pathways involved in its pathogenesis. This study aims to elucidate the pathogenesis of IGT and provide new insights and evidence for understanding its molecular basis and for future intervention therapy. The structure of our paper is shown in Fig. 1.

Results

Blood glucose levels in the IGT rats

This study conducted an OGTT test on both Ctrl group ($n=6$) and IGT group ($n=6$) rats on day 0 and day 42 after the IGT group was established, the results were shown in Fig. 2A-B. Obviously, the glucose concentration in the IGT group was significantly higher than the Ctrl group on both day 0 ($P=0.0013$) and day 42 ($P<0.0001$) after a 120-min post-load glucose challenge.

Overview of transcriptome analysis

We compared the IGT and Ctrl samples to identify target genes relevant to this study. The standard and unique genes of the two groups were visualized. The Venn diagram was drawn as follows (Fig. 3A). There were 10,832 co-expressed genes in total, accounting for 92.2%, 436 unique genes in the Ctrl group, accounting for 3.71% and 481 unique genes in the IGT group, accounting for 4.09%. Principal component analysis (PCA) (Fig. 3B) showed that the IGT and Ctrl groups were highly similar within each group, and the two groups showed clear discrimination.

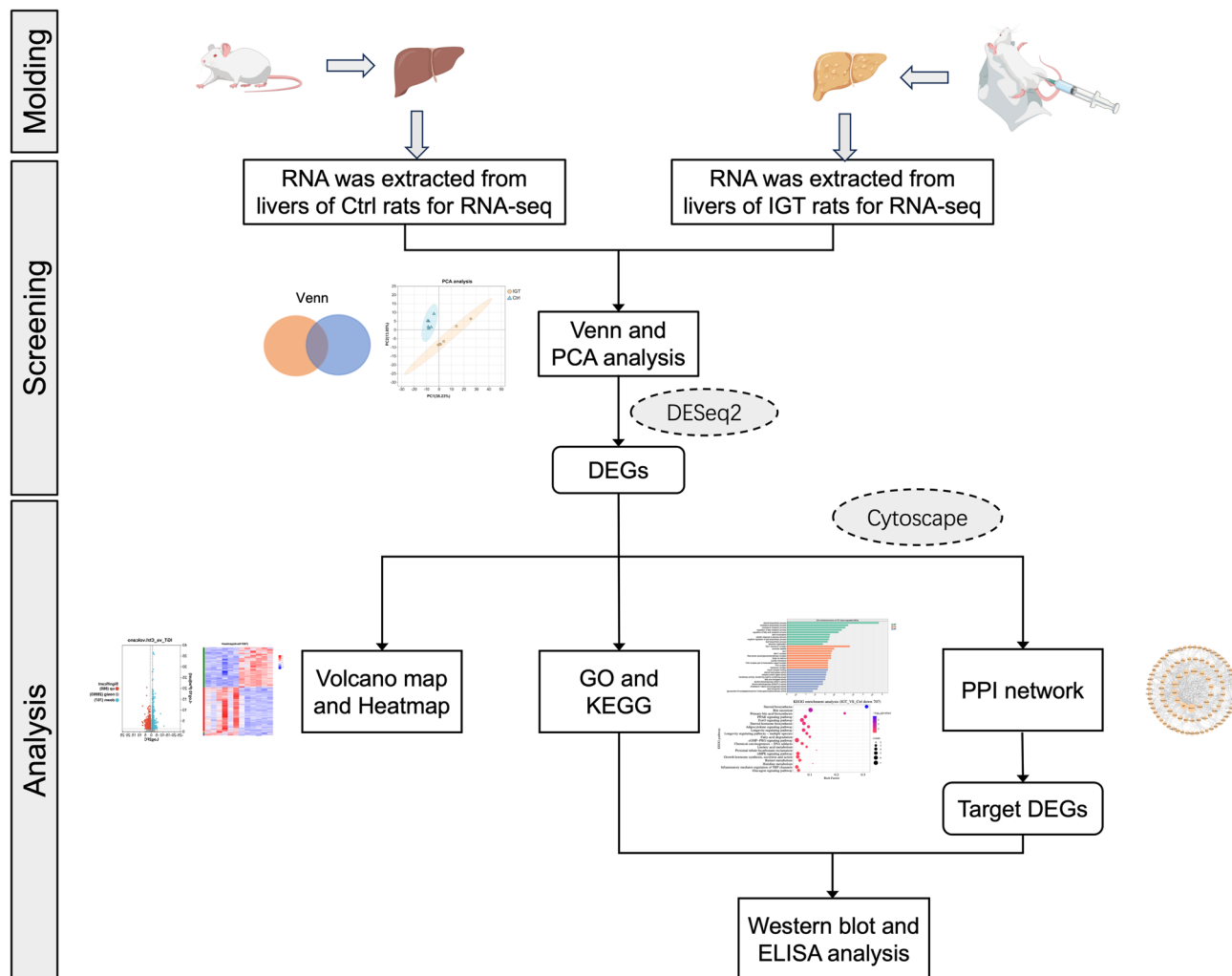


Fig. 1. The workflow of this study.

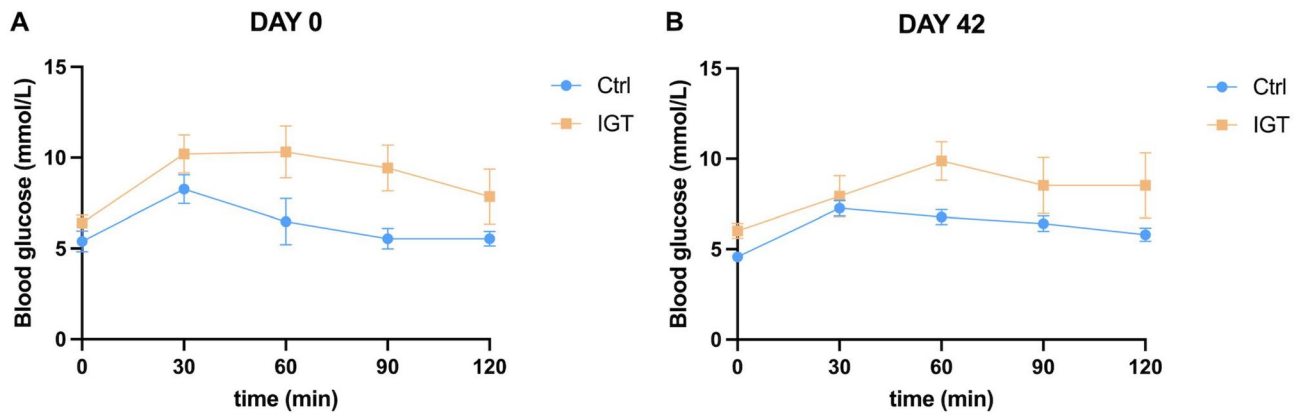


Fig. 2. Blood glucose levels of day 0 and day 42 in the IGT and Ctrl group ($n=6$ per group). Values are presented as mean \pm SD. When comparisons were made between the Ctrl and IGT groups #, $P<0.05$, ##, $P<0.01$, ####, $P<0.0001$.

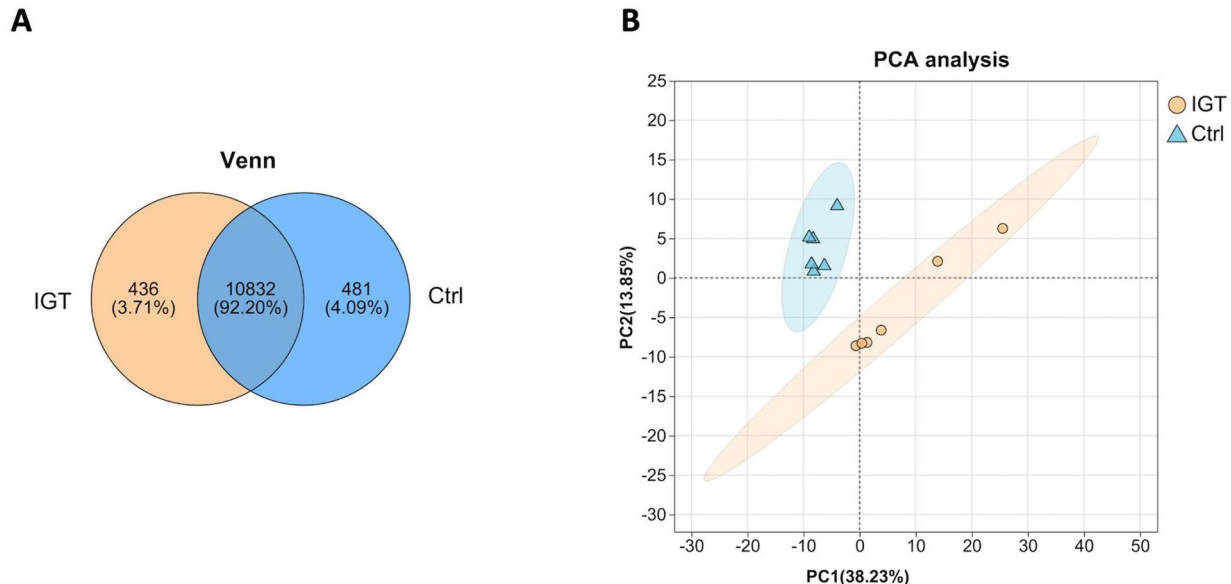


Fig. 3. Results of analysis between the IGT and Ctrl group. (A) Venn diagram. (B) PCA analysis.

Screening of DEGs

Through the analysis and identification of genes in the IGT and Ctrl groups, a total of 1567 differentially expressed genes (DEGs) were identified, of which 860 genes were up-regulated and 707 genes were down-regulated. To visualize the differential gene expression, we constructed a volcano map (Fig. 4A) and a heat map (Fig. 4B-C) based on our RNA-seq results. In the volcano map, genes with significant fold changes in differential expression appear on the left and right sides of the midline, respectively, while significantly expressed DEGs appear higher in the plot. The heat map illustrated the clustering gene expression across multiple samples, with red indicating significant up-regulation and blue indicating substantial down-regulation. The results suggested significant differences between the IGT and the Ctrl groups. Notably, the supplementary table provides the entire list of 1567 DEGs (Supplementary Material. S1).

Enrichment analysis of DEGs

GO enrichment analysis of DEGs

GO enrichment analysis was performed on the up- and down-regulated DEGs across three categories: biological process (BP), cellular component (CC), and molecular function (MF), respectively, with a significance threshold of p -value <0.05 . The results were shown in Fig. 5A,B.

In biological processes, up-regulated genes were mainly enriched in the regulation of interleukin-1 beta (IL-1 β) production, regulation of interferon-gamma (IFN γ) production, cellular response to IFN γ , regulation of I-kappaB kinase/NF-kappaB (NF- κ B) signaling, positive regulation of IFN γ production and positive regulation

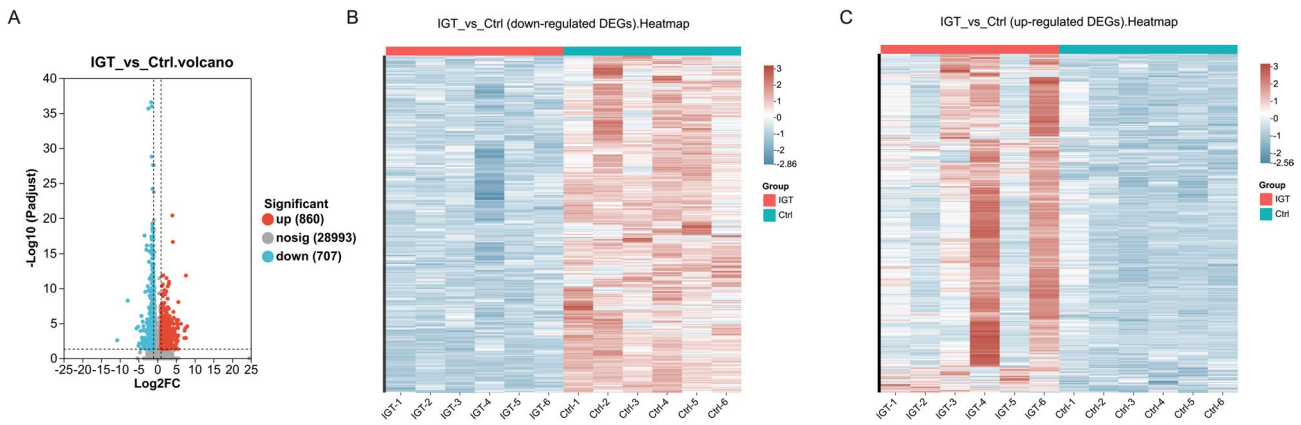


Fig. 4. Differential expression analysis of RNA-seq. (A) Volcano map. The x-axis (log2FC) represents the fold change in gene expression difference between the IGT and Ctrl group after log transformation. The larger the absolute value, the greater difference in gene expression between the two groups. Positive value indicates that the difference is up-regulated, while negative value indicates that the difference is down-regulated. The y-axis represents the significance gene expression changes, where a smaller Padj indicates a more substantial difference. Red dots indicate significantly up-regulated genes, blue dots indicate significantly down-regulated genes, and gray dots indicate non-significant genes. (B,C) Heat map. Each column represents a sample, each row represents a gene, and the color in the figure indicates the magnitude of gene expression in each sample. Red indicates higher gene expression in that sample, while blue indicates the opposite.

of IL-6 production. Down-regulated genes were mainly enriched in the steroid biosynthetic process, cholesterol biosynthetic process, cholesterol metabolic process, regulation of lipid metabolic process, and regulation of fatty acid metabolic process.

For cellular components, up-regulated genes were primarily associated with MHC protein complex, immunological synapse, lytic vacuole, lysosome, and plasma membrane signaling receptor complex. Down-regulated genes were primarily associated with Ssh1 translocon complex, centriolar satellite, axon, Mre11 complex, and Rab-protein geranylgeranyltransferase complex.

In molecular function, up-regulated genes were mainly enriched in chemokine activity, chemokine receptor binding, cytokine receptor activity, cytokine binding, and immune receptor activity. Down-regulated genes were mainly enriched in insulin receptor binding, steroid hydroxylase activity, alcohol dehydrogenase (NAD+) activity, alcohol dehydrogenase [NAD(P)+] activity, and cholesterol 7-alpha-monoxygenase activity. Specific GO enrichment details are provided in the Supplementary Materials (Supplementary Material. S2).

KEGG enrichment analysis of DEGs

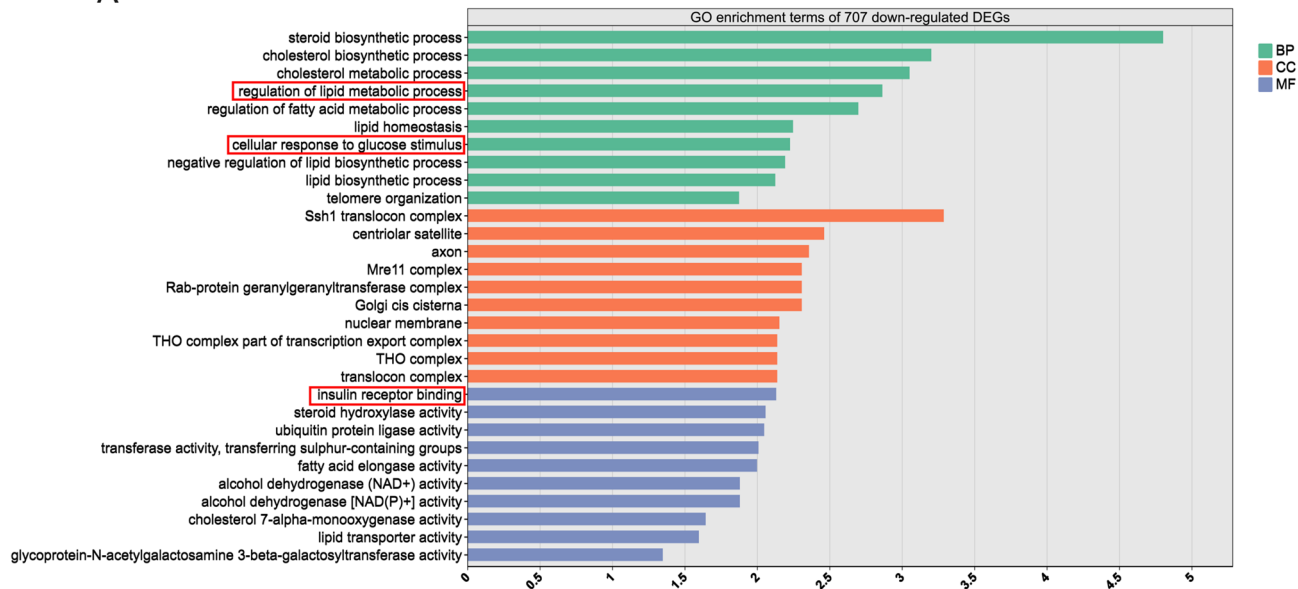
According to the pathway significance ($p\text{-value} < 0.05$), the top 20 KEGG enrichment analysis for the 860 up-regulated DEGs were shown in the bubble chart (Fig. 6A). The results show that up-regulated DEGs were mainly involved in Antigen processing and presentation, Cytokine-cytokine receptor interaction, chemokine signaling pathway, NF- κ B signaling pathway, Cell adhesion molecules, Osteoclast differentiation, Allograft rejection, NOD-like receptor signaling pathway, Th1 and Th2 cell differentiation and Natural killer cell mediated cytotoxicity.

Similarly, based on the pathway significance $p\text{-value}$, the top 20 of the KEGG enrichment analysis for the 707 down-regulated DEGs were shown in the bubble chart (Fig. 6B). The results show that down-regulated DEGs were mainly enriched with Steroid biosynthesis, Bile secretion, Primary bile acid biosynthesis, PPAR signaling pathway, FoxO signaling pathway, Steroid hormone biosynthesis, Adipocytokine signaling pathway, Longevity regulating pathway, Longevity regulating pathway-multiple species and Fatty acid degradation. Specific KEGG enrichment pathways are presented in the Supplementary Materials (Supplementary Material. S3).

Construction and analysis of the PPI network

This study utilized the online analysis database “STRING 12.0” to further investigate the function of genes at the protein level. Using the up-regulated and down-regulated DEGs as target genes, respectively, we retrieved the interactions between gene expression proteins, set the minimum interaction confidence score to 0.400, and constructed the respective DEGs’ protein-protein interaction (PPI) networks. In these networks, nodes represent proteins, and connections represent interactions between proteins. The interaction files exported from STRING were visualized in Cytoscape (3.9.1). The PPI core network for the up- and down-regulated DEGs was analyzed using Betweenness (BC) in the CytoNCA plug-in, and each DEG was assigned a value based on a topological net algorithm. The top 10 DEGs were sorted and screened to construct a subnetwork and identify key nodes.

A



B

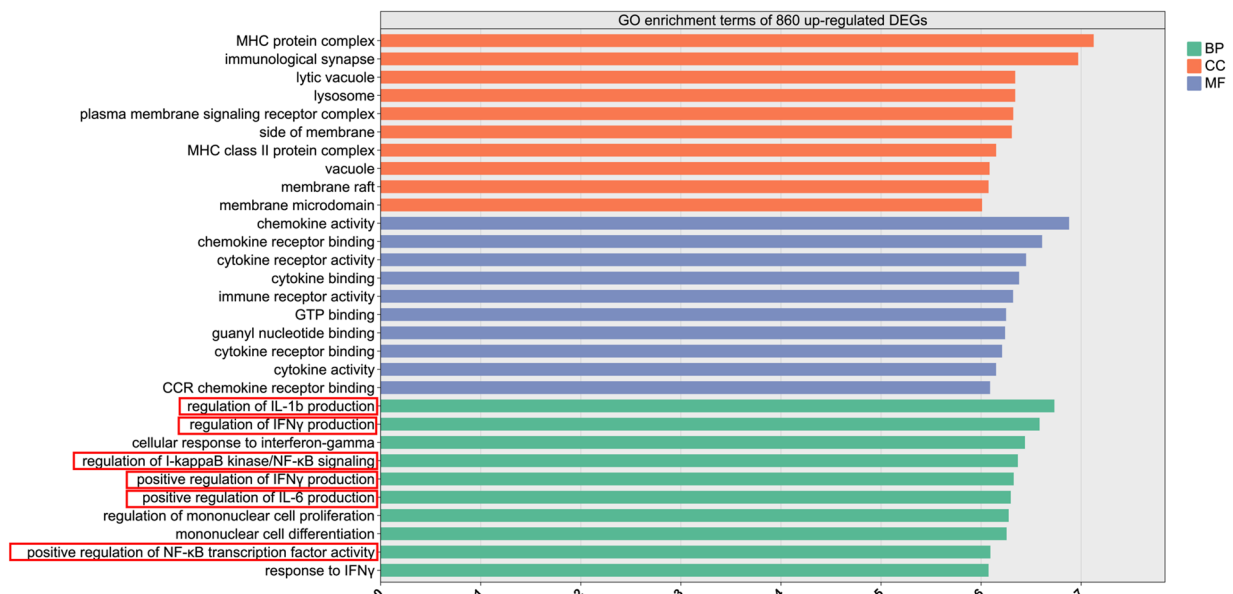


Fig. 5. Histogram of GO enrichment analysis. (A) GO enrichment terms of 707 down-regulated DEGs of IGT vs. Ctrl. (B) GO enrichment terms of 860 up-regulated DEGs of IGT vs. Ctrl.

PPI network construction of up-regulated DEGs and screening of top 10 DEGs

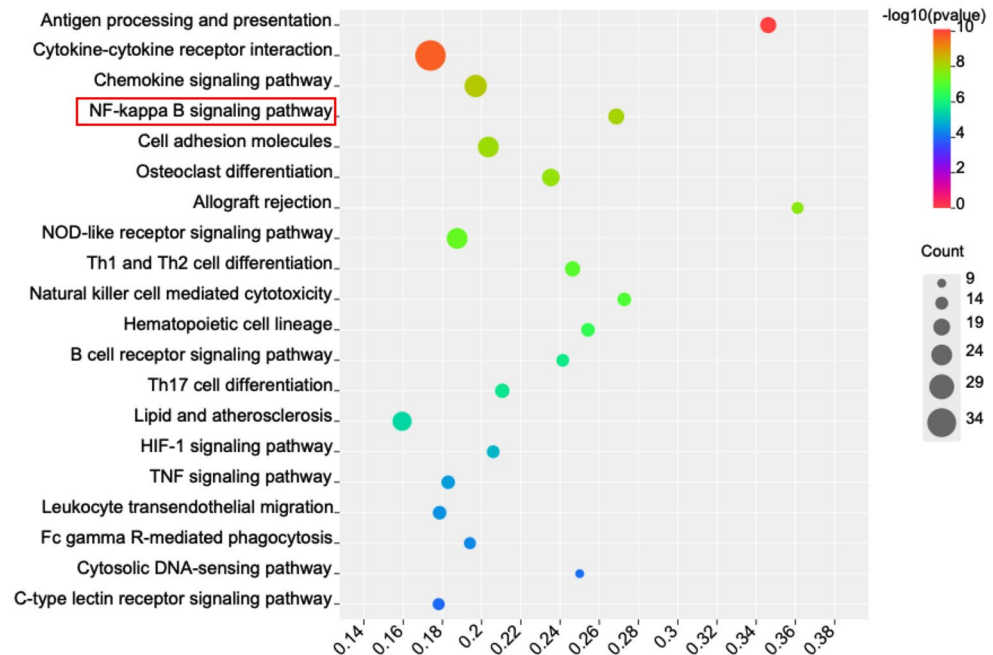
A PPI network of the up-regulated DEGs was constructed using visualization software, forming a complex network consisting 787 nodes and 6343 lines. The top 100 DEGs based on betweenness centrality score were extracted and ranked to generate the PPI network diagram (Fig. 7A). The top 10 DEGs were screened and used to construct the sub-network, as shown in Fig. 7B. These top 10 DEGs, *IL-1 β* , *Cd44*, *Tyrobp*, *Stat1*, *Cd74*, *Rac2*, *Lck*, *Icam1*, *Cdk1* and *Itgad*, were identified as possible core nodes in the up-regulated DEGs network.

PPI network construction of down-regulated DEGs and screening of top 10 DEGs

The PPI network of down-regulated DEGs was similarly constructed, forming a network of 473 nodes and 577 lines. The top 100 DEGs based on betweenness centrality score were extracted and ranked to create the PPI network diagram (Fig. 7C). The top 10 DEGs were screened to construct the sub-network, as shown in Fig. 7D. These top 10 DEGs, *Mysm1*, *Igf-1*, *Smc5*, *Nipbl*, *Cyp7a1*, *Amdhd1*, *Atrx*, *Ranbp2*, *Xiap*, and *Gfra1*, were identified as possible core nodes in the down-regulated DEGs network.

A

KEGG enrichment analysis (IGT_VS_Ctrl up 860)

**B**

KEGG enrichment analysis (IGT_VS_Ctrl down 707)

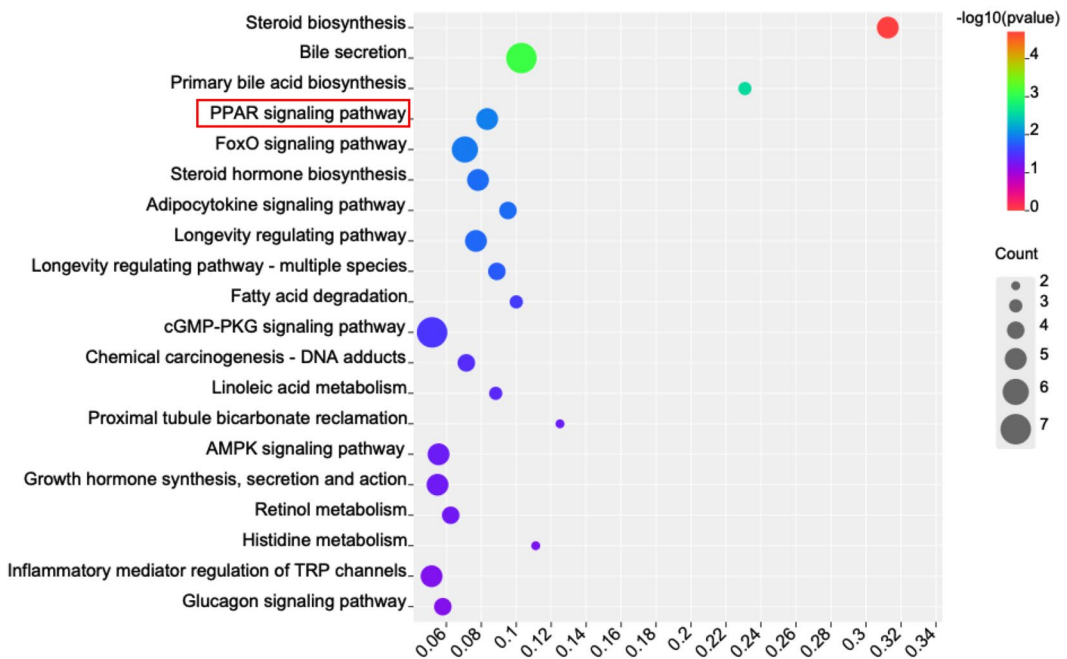


Fig. 6. KEGG enrichment bubble chart. In the bubble chart, we sorted the top 10 pathways by p-value and visualized them; the darker the node in the graph, the higher the ranking. (A) The top 20 enrichment signaling pathways of 860 up-regulated DEGs in IGT vs. Ctrl. (B) The top 20 enrichment signaling pathways of 707 down-regulated DEGs in IGT vs. Ctrl. The Kyoto Encyclopedia of Genes and Genomes (KEGG) pathway map was obtained from KEGG (<https://www.kegg.jp/>). KEGG is a publicly available resource under the terms of the academic uselicense^{13,14}.

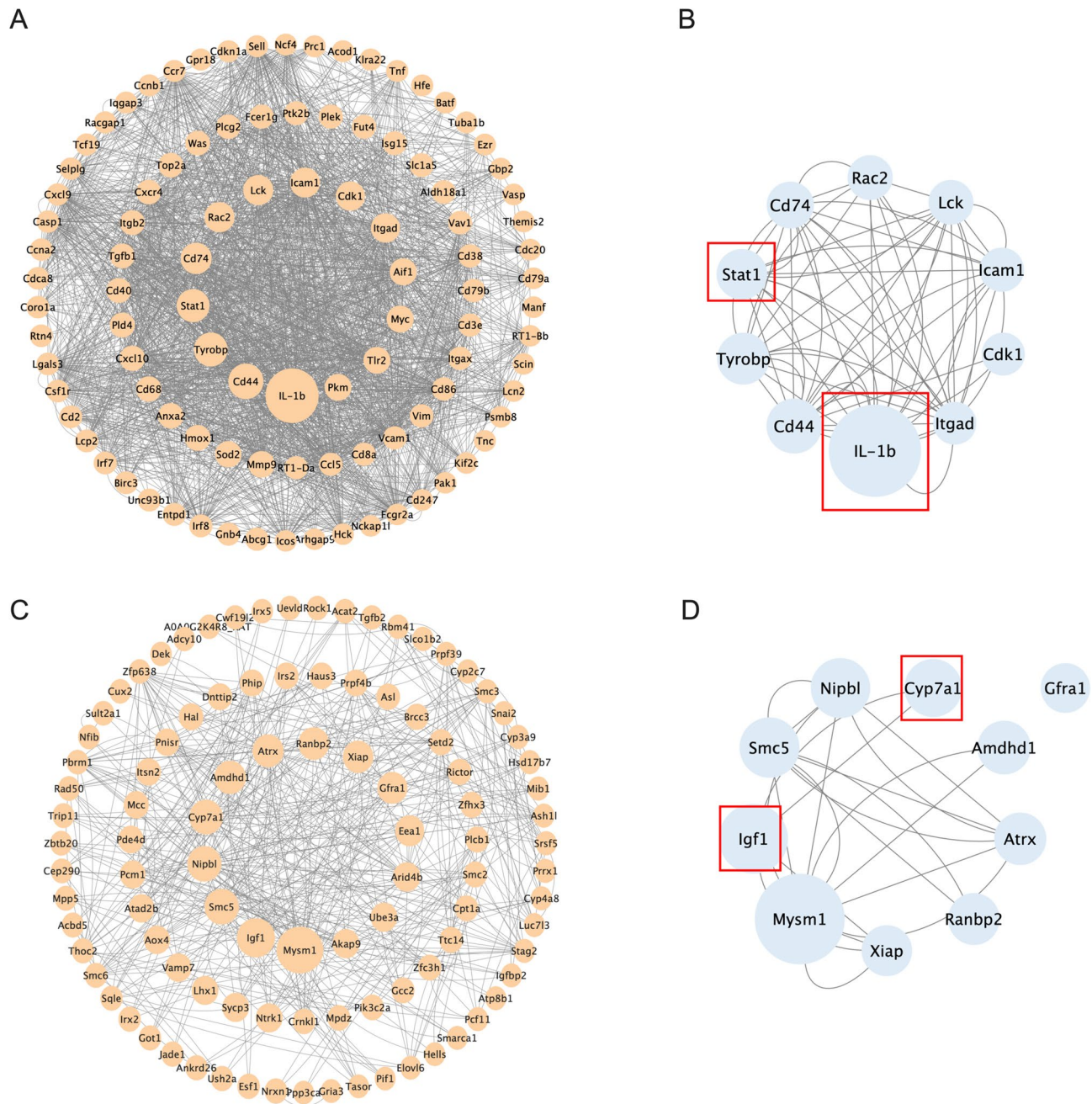


Fig. 7. (A) The PPI network module is composed of the top 100 up-regulated DEGs. (B) The PPI network module is composed of the top 10 up-regulated DEGs. (C) The PPI network module is composed of the top 100 down-regulated DEGs. (D) The PPI network module is composed of the top 10 down-regulated DEGs.

To further elucidate the pathogenesis of IGT, as per the top 10 DEGs identified through the above transcriptome analysis. Based on literature review and experimental data, we hypothesized that *IL-1b*, *Stat1*, *Igf-1*, and *Cyp7a1* may be Target DEGs (T-DEGs) that play a critical regulatory role in the pathogenesis of IGT. These selected T-DEGs are associated with the NF- κ B and PPAR signaling pathways identified in KEGG enrichment analysis.

In this study, PPAR γ was decreased in the IGT group compared to the Ctrl group, as shown in Supplementary Material, S4. Consistent with this, previous research has demonstrated two primary mechanisms. In adipocytes, Kyle et al. reported that PPAR γ is a target gene of STAT1. p-STAT1 binds to the IFN- γ response element in the PPAR γ promoter region, directly suppressing its transcription¹⁵. In macrophages, IFN- γ stimulation induces STAT1 phosphorylation (p-STAT1)¹⁶, which promotes M1 macrophage polarization¹⁷, thereby reducing M2 populations and inhibiting PPAR γ activity¹⁸. This process diminishes the antagonistic effect on NF- κ B signaling, exacerbating the inflammatory response¹⁶. These observations strongly align with the potential inflammatory state in IGT and underscore the critical role of the STAT1/PPAR γ balance in disease pathogenesis. Therefore, we propose that during the pathogenesis process of IGT, *Stat1* down-regulates *Ppary* in the PPAR-related pathway,

further leading to alterations in genes such as *IL-1b*, *Igf-1*, and *Cyp7a1*. Concurrently, changes in the NF- κ B signaling pathway and elevated inflammation-related factors induce inflammatory responses and alter blood glucose levels. To validate this hypothesis, we conducted biological experiments to verify these related genes.

Western blot analysis

Western blot results verified the genes related to our conjecture at the expression levels of three proteins (Fig. 8). Compared with the Ctrl group, the expression of PPAR γ ($P=0.0022$) was lower in the IGT group. Since the transcriptional activity of NF- κ B is regulated by phosphorylation or complete activation of acetylation of the p65 subunit, detection of p65 using protein validation is an indispensable indicator for studying the NF- κ B signaling pathway. The results revealed that p65 ($P<0.0001$) was higher in the IGT group than in the Ctrl group. Furthermore, the hub gene *Stat1* regulatory protein undergoes phosphorylation, leading to the formation of p-STAT1. The results showed that the expression level of p-STAT1/ STAT1 protein was significantly elevated in the IGT group compared to the Ctrl group ($P<0.0001$). These results are consistent with our hypothesis. Collectively, our findings suggest that STAT1 may act as a negative regulator of PPAR γ in the context of IGT. Please be informed that the original and uncropped blots corresponding to Fig. 8A are provided in the Supplementary file (Supplementary Material. S5).

Inflammatory cytokines level in the IGT rats

Based on the above Western blot verification, we believe that phosphorylation and activation of Stat1 in IGT may affect PPAR γ expression, leading to reduced PPAR γ levels. To further investigate whether inflammatory cytokines play a role in this process, we selected four factors, including the differential gene IL-1 β , and analyzed their levels in rat serum. The results are shown in Fig. 9. Compared with the Ctrl group, the levels of IFN γ

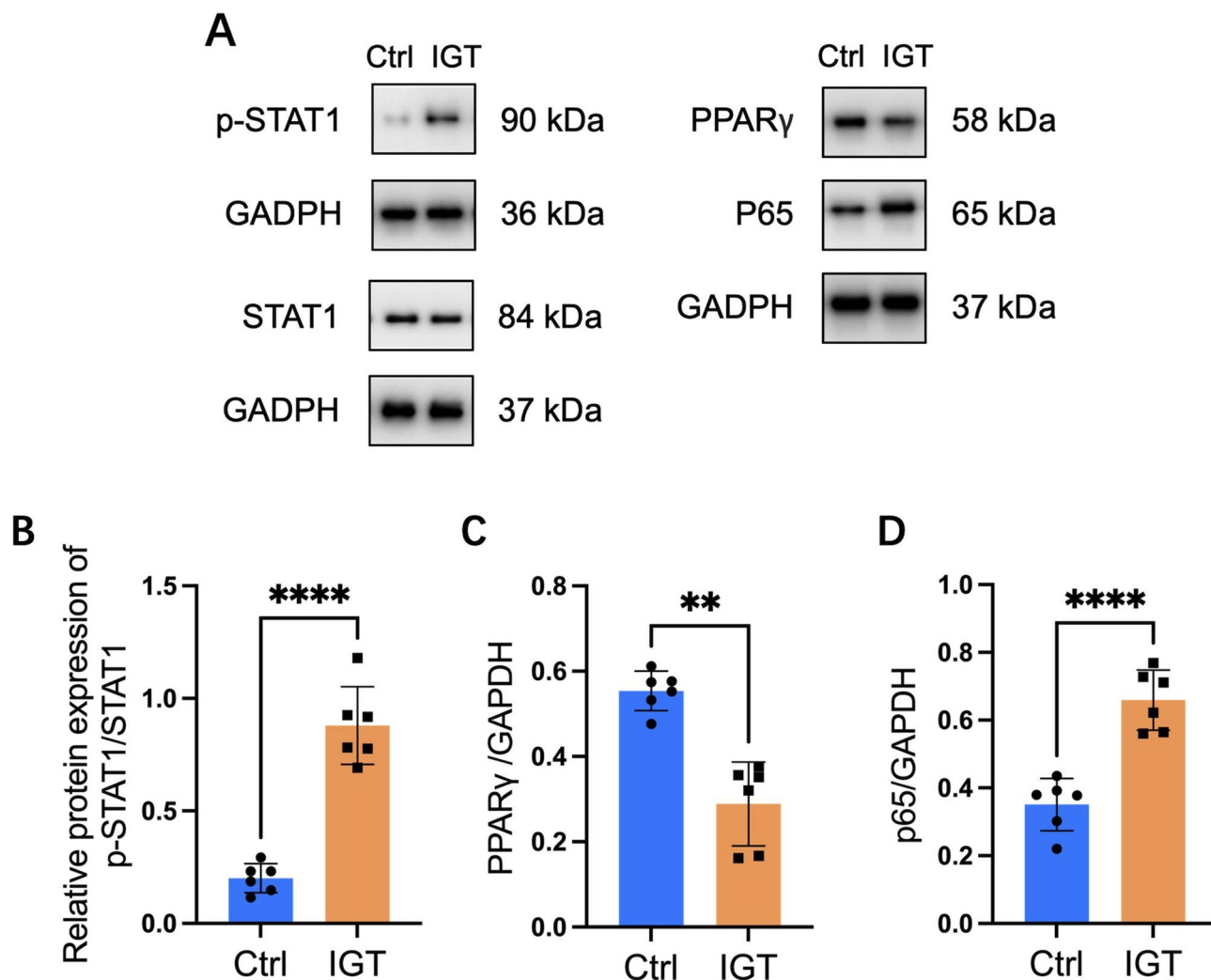


Fig. 8. Western blot. (A) A summary graph for quantitative analysis of p-STAT1, STAT1, p65, and PPAR γ protein densitometry. (B–D) Relative protein expression of p-STAT1/STAT1, PPAR γ , and p65. When comparisons were made between the Ctrl and IGT groups, graphs represent mean \pm SD. #. $P<0.05$, ##. $P<0.01$, ####. $P<0.0001$.

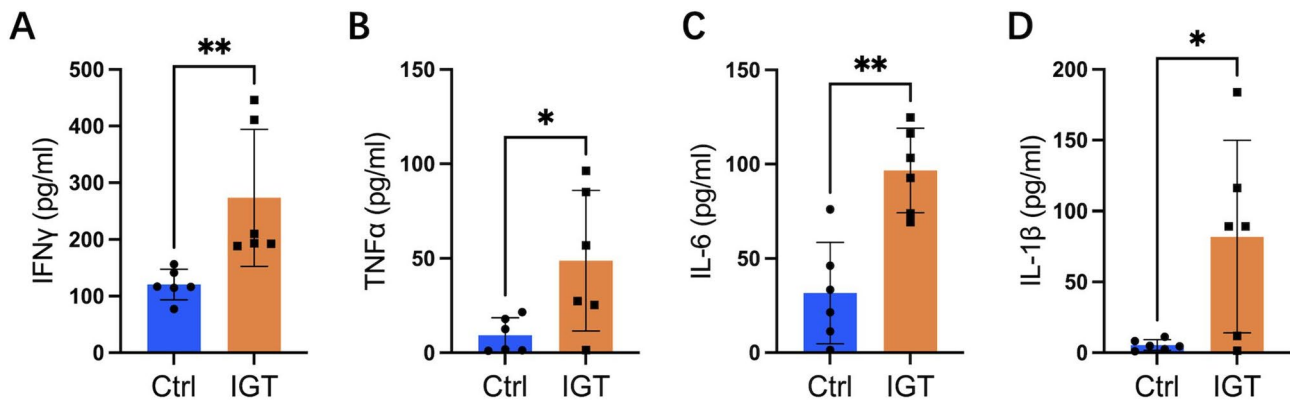


Fig. 9. Compared with the Ctrl group, the serum levels of IFN γ , TNF α , IL-6, and IL-1 β in the IGT group. When comparisons were made between the Ctrl and IGT groups, graphs represent mean \pm SD. #. $P < 0.05$, ##. $P < 0.01$, ####. $P < 0.0001$.

($p = 0.0022$), TNF α ($p = 0.0303$), IL-6 ($p = 0.0011$), and IL-1 β ($p = 0.037$) in IGT group were significantly elevated. This study has shown that the levels of inflammatory cytokines in IGT rats have improved considerably, suggesting excessive activation of the inflammatory response, which may contribute to the development and progression of the disease.

Discussion

The pathogenesis of IGT is closely associated with glucose metabolism disorders and is related to the degree of obesity and abnormal lipid metabolism. Research indicates that^{19,20}, compared to the normoglycemic population, both obesity and dyslipidemia are more prevalent in the IGT group. Obesity is an independent risk factor for T2DM, and the dyslipidemia pattern in IGT resembles that of the T2DM population. These risk factors can promote adipose tissue inflammation, thereby accelerating the progression from IGT to T2DM. However, the intrinsic molecular mechanisms underlying their interaction in IGT pathogenesis remain unclear, limiting advancements in early T2DM prevention and treatment.

In the study, an IGT rat model was established to investigate the pathogenesis of IGT and to provide evidence for its early prevention and treatment. Transcriptomic analysis was performed to identify key genes and signaling pathways involved in IGT progression. Finally, a total of 1567 DEGs were identified, including 860 up-regulated and 707 down-regulated genes. Among these, *IL-1b*, *Stat1*, *Igf-1*, and *Cyp7a1* were identified as T-DEGs. Based on our data, we hypothesize that STAT1/PPAR γ /IGF-1, STAT1/PPAR γ /Cyp7a1, and STAT1/PPAR γ /IL-1 β pathways may play key roles in the pathogenesis of IGT.

The IGT pathogenesis process involves multiple transcriptional pathways. PPAR (peroxisome proliferator-activated receptor) includes subtypes PPAR α , PPAR β/δ , and PPAR γ . As a transcription factor activated by endogenous ligands, PPAR plays a central role in glucose regulation, inflammation response, and cell differentiation. Previous studies have demonstrated its crucial role in glucose metabolism in T2DM^{21,22}. In particular, PPAR γ promotes adipocyte differentiation, enhances insulin sensitivity, regulates adipogenesis and maintains the function of mature adipocytes²³. Given its pivotal role, PPAR γ is an important therapeutic target for T2DM, and its agonists are widely used in diabetes treatment²².

Impaired glucose uptake in adipose tissue can disrupt glucose metabolism. PPAR γ plays a key role in promoting adipocyte differentiation, and its down-regulation can impair adipocyte differentiation and thereby glucose uptake. Transcriptional inhibition of PPAR γ reduces the ability of mesenchymal progenitor cells to differentiate into the adipocyte lineage, resulting in fewer nascent adipocytes. Nascent adipocytes are critical for altering adipose tissue function. The reduction in newly differentiated adipocytes exacerbates the dysfunction of existing adipose tissue, decreasing glucose uptake and increasing the risk of metabolic disorders and impaired glucose tolerance²⁴. Previous analyses related to T2DM have confirmed that STAT1 is a major transcription factor regulating diabetes pathogenesis²⁵. In this research, as early as the IGT stage, STAT1 was up-regulated in the IGT group compared to the Ctrl group. This up-regulation may inhibit adipocyte differentiation through the PPAR γ signaling pathway. A study has shown that STAT1 mediates IFN γ induced inhibition of adipocyte differentiation²⁶. Further study revealed that STAT1 and IFN γ can influence PPAR γ transcription. Increased IFN γ expression may directly modulate adipocyte differentiation by up-regulating activated STAT1, which binds to the IFN γ site within the PPAR γ promoter and induces its transcriptional repression²⁷. Moreover, abnormal adipocyte hypertrophy reduces adipose tissue's capacity to store excess lipids, thereby increasing the risk of glucose metabolic disorders and impairing glucose uptake²⁸. Lipoprotein lipase (LPL) is a key enzyme that hydrolyzes triglycerides into free fatty acids for uptake and storage in adipose tissue. While PPAR γ induces LPL gene expression, STAT1 may directly suppress LPL by binding to its promoter. Down-regulation of LPL activity leads to triglyceride accumulation, resulting in enlarged lipid droplets, adipose tissue expansion, and adipocyte hypertrophy. These alterations collectively contribute to impaired glucose homeostasis^{27,29,30}.

In this study, transcriptomic analysis revealed that PPAR γ decreased in the IGT group compared to the Ctrl group, although the difference did not reach statistical significance. Specifically, transient sampling during

sequencing may have failed to capture the temporal or cell-type-specific down-regulation of PPAR γ expression. In the context of IGT, PPAR γ down-regulation may vary across cell types, such as adipocytes or macrophages, or across particular disease stages. Since this study analyzed liver tissue, these critical localized changes may not have been fully captured. Moreover, the PPAR γ gene produces multiple transcript isoforms³¹. The RNA-seq used here may preferentially detect the more abundant isoforms, while underrepresenting low-expression, disease-sensitive variants. These isoforms may contribute to the discrepancies observed between transcriptomic and proteomic data. Research indicates³² that PPAR $\gamma\Delta 5$, a natural splicing isoform generated by exon 5 skipping, lacks a complete ligand-binding domain. Under hyperglycemic conditions, particularly in obese individuals, ligand-activated PPAR γ can induce exon 5 skipping, leading to PPAR $\gamma\Delta 5$ formation and establishing a negative feedback loop. This process increased the PPAR $\gamma\Delta 5$ /PPAR γ ratio, thereby reducing the functional PPAR γ level. This mechanism may partly explain the reduction in PPAR γ protein expression observed in IGT. Furthermore, PPAR $\gamma\Delta 5$ retains the ability to interact with RXR α , which impairs PPAR γ 's regulatory capacity. Elevated PPAR $\gamma\Delta 5$ in adipose tissue disrupts the PPAR γ gene network, leading to variant formation, function loss, and impaired adipocyte differentiation. It is important to note that this study has certain limitations. Although the PPAR γ expression change was confirmed at the protein level by Western blot, qPCR validation was not performed due to experimental constraints. As a result, the RNA-seq data lack additional experimental support. Further verification using qPCR and other approaches will be carried out in future work.

Previous studies have demonstrated that IR emerges during the IGT stage³³. Fat tissue is crucial for maintaining insulin sensitivity. Macrophages promote glucose uptake in adipocytes, regulate lipid homeostasis, and increase energy expenditure, thereby supporting metabolic homeostasis³⁴.

Firstly, our study found that decreased PPAR γ may hinder the polarization of M2 macrophages, thereby facilitating IR^{35,36}. In diverse microenvironments, macrophages can be classified into classically activated macrophages (M1 macrophages) and alternatively activated macrophages (M2 macrophages) based on their polarization phenotypes. It is generally considered that M1 macrophages exert pro-inflammatory functions, whereas M2 macrophages exert anti-inflammatory functions³⁷. In comparison, a reduction in M2 macrophages diminishes their ability to maintain insulin sensitivity³⁸. The up-regulated PPAR γ signaling pathway plays a crucial role in facilitating M2 polarization of macrophages³⁹. The research found that STAT1 is a key factor in inhibiting the transcription of the macrophage regulator PPAR γ ^{17,40}. Therefore, STAT1/PPAR γ inhibits M2 polarization of macrophages and maintains the M1 phenotype, which may be the mechanism underlying decreased insulin sensitivity and elevated serum glucose.

Secondly, our research found that IGF-1 expression was significantly down-regulated in the IGT group compared with the Ctrl group. KEGG pathway enrichment analysis suggested that IGF-1 may contribute to the down-regulation of PPAR γ expression in IGT through the FOXO pathway. Previous studies have shown that decreased IGF-1 correlates with increased M1 macrophages⁴¹. IGF-1 and insulin share identical downstream signaling pathways and are involved in the uptake of glucose and fatty acids in peripheral tissues, thereby regulating glucose homeostasis. It is a risk factor for progression from standard glucose tolerance to IGT⁴². Down-regulation of IGF-1 facilitates the functional effects of the FOXO transcription factor. In the FOXO signaling pathway, IGF-1 combines with the IGF-1 receptor (IGF-1R), activates IRS, and promotes Akt phosphorylation via the PI3K-Akt signaling pathway. This, in turn, stimulates FOXO phosphorylation, inhibiting FOXO nuclear entry and suppressing its function. Additionally, FOXO1, a FOXO family member, binds to the PPAR γ promoter, suppressing its expression and influencing metabolic regulation⁴³. When IGF-1 expression is down-regulated, IGF-1 and IGF-1R interaction is reduced, attenuating FOXO functional inhibition, leading to reduced PPAR γ expression and macrophage recruitment⁴⁴. During IGT pathogenesis, M1-like accumulation macrophage is a marker of elevated blood glucose. Changes in macrophage polarization caused by STAT1/PPAR γ are associated with altered IGF-1 levels. This STAT1/PPAR γ /IGF-1 inhibitory mechanism may further decrease PPAR γ expression, exacerbating IR and increasing blood glucose levels.

Thirdly, Cyp7a1 is involved in macrophage cholesterol efflux of the PPAR γ pathway, which influences glucose metabolism. Studies have shown that decreased PPAR γ expression reduces liver X receptor α (LXR α) expression, attenuating the PPAR γ /LXR α /Cyp7a1 pathway⁴⁵. Cyp7a1, activated downstream of the PPAR γ /LXR α pathway, encodes cholesterol 7 α -hydroxylase in the liver, the first rate-limiting enzyme in bile acid synthesis, which catalyzes cholesterol transformation⁴⁶. When PPAR γ /LXR α is down-regulated, Cyp7a1 activation is restricted, disrupting cholesterol metabolism and leading to cholesterol deposition. This also reduces bile acid synthesis. Bile acid-activated farnesoid X receptor (FXR) enhances insulin sensitivity. Its decreased activity facilitates IR, glucose metabolism disorders, and elevated blood glucose levels⁴⁷. In this study, Cyp7a1 expression was significantly down-regulated in the IGT group compared to the Ctrl group. This finding is consistent with the results from the aforementioned studies, indicating that Cyp7a1 may play a critical role in the progression of IGT.

Fourthly, previous studies have indicated that IL-1 β transcription levels are markedly elevated in patients with IGT and even in the T2DM population⁴⁸, and that these levels are associated with obesity and contribute to the development of IR⁴⁹. IL-1 β also influences macrophage polarization, its excessive release from macrophages induces classical M1 macrophage activation⁵⁰. This aligns with the blockade of the STAT1/PPAR γ pathway, suggesting its role in promoting M1 macrophages and affecting the FOXO signaling pathway. Consequently, the IRS/Akt/FOXO1 signaling pathway is activated, leading to increased FOXO1 phosphorylation. As a transcription factor, FOXO1 further enhances IL-1 β ⁵¹. Conversely, PPAR γ 's anti-inflammatory effects are well-documented⁵². PPAR γ activation can restrain IL-1 β inflammation. In the IGT inflammatory state, TNF- α and IL-1 β further enhance NF- κ B mediated suppression of PPAR γ expression. This hinders the anti-inflammatory capacity of PPAR γ , perpetuating the inflammatory environment^{23,53}. The increased IL-1 β expression further complicates the resolution of inflammation, making the inflammatory state increasingly persistent and challenging to reverse. Additionally, IL-1 β also inhibits the Cyp7a1 transcription via the c-Jun-N-terminal kinase/c-Jun pathway,

thereby facilitating IR⁵⁴. Similarly, IL-6 and TNF- α disrupt insulin signalling and insulin-stimulated glucose uptake, leading to elevated blood glucose levels⁵⁵. In this study, Western blot and ELISA analysis revealed that the primary factor NF- κ B p65, which regulates immune-mediated inflammatory responses, was significantly elevated in IGT group rats compared to rats with normal blood glucose. Additionally, the secretion levels of inflammatory cytokines including TNF α , IL-6, and IL-1 β were significantly increased. These results indicate that inflammatory cytokines are abnormally activated as early as the IGT stage, thereby promoting IR and glucose metabolism disorders.

Furthermore, PPI analysis indicates that although no significant associations were found between the other top 10 DEGs and the PPAR signaling pathway, these genes may still influence lipid metabolism or inflammation. This requires further investigation. Itgad (CD11D) mediates inflammatory signal transduction and macrophage recruitment. Highly expressed in adipose tissue macrophages, Itgad enhances the infiltration and retention of M1 macrophages in adipose tissue, intensifying macrophage inflammatory signal^{56,57}. Additionally, highly expressed Tyrobp is associated not only with chemokine activation but also with the regulation of IL-1 β and IL-6. However, also related to JAK/STAT pathway activation, increasing inflammation-related levels. Tyrobp induces macrophage polarization and the pro-inflammatory NK cell response, leading to chronic adipose inflammation and dysfunction^{58,59}. Importantly, the findings presented in this study are not limited to the T-DEGs identified but may also encompass certain other DEGs with potential research value and significance. These results provide an experimental basis for future IGT studies, and the potential roles of these genes warrant further exploration.

Conclusion

This study compared transcriptome differences between the healthy and IGT rats. Using bioinformatics techniques, quantitative and functional analyses were conducted, and a gene regulatory network was constructed. *IL-1b*, *Stat1*, *Igf-1*, and *Cyp7a1* were identified as T-DEGs. The findings revealed that as early as the IGT period, these T-DEGs may mediate the onset and progression of IGT via the PPAR γ signaling pathway. Additionally, potential regulatory networks were identified, including STAT1/PPAR γ /IGF-1, STAT1/PPAR γ /Cyp7a1, and STAT1/PPAR γ /IL-1 β .

Methods

Ethics declarations

The animal experiment research was approved by the Ethics Committee for Animal Experiments of Beijing University of Chinese Medicine (Ethics No.: BUCM- 2023041911-2127). All experiments were performed in accordance with the Regulations for the Administration of Experimental Animals issued by the State Council of China in 2017. All authors complied with the ARRIVE guidelines.

Animals and sample collection

Twenty 6-week-old SPF-grade male Sprague-Dawley rats were purchased from Charles River Laboratory Animal Co., LTD. (Beijing, China). All the rats weighed 200 g \pm 20 g. Laboratory Animal Qualification License No.: SCXK2021-0006.

The 20 purchased rats were routinely housed in separate cages at the SPF Experimental Animal Center of Beijing University of Chinese Medicine, where the temperature was maintained at 18–22°C and the relative humidity at 30–70%. The laboratory followed a 12-hour circadian cycle. All experimental animals had free access to diet and water to help them adapt to the new experimental environment. After one week of adaptive feeding, 6 of the 20 rats were randomly selected for the Ctrl group and fed an ordinary diet. The remaining 14 rats were fed a high-fat diet to establish the IGT model. After 21 days of feeding, rats in both groups were fasted for 12 h. The IGT model was induced via intraperitoneal injection with STZ (Streptozotocin, Sigma, Germany) dissolved in 1% sodium citrate buffer (0.1 mol/L, pH4.5) at a dose of 18 mg/kg^{60,61}. The Ctrl group was injected intraperitoneally with normal saline (0.9% sodium chloride) (1 ml/100 g). On the third day after the end of the injection procedure, rats in both groups were fasted for 12 h and then given a 50% glucose solution (1 ml/100 g) via intragastric administration. Tail vein puncture was performed at 0, 30, 60, 90, and 120 min after gavage, and a glucose meter (Abbott Laboratories, CHI, USA) was used to measure and record blood glucose levels in rats. IGT modeling was considered successful when blood glucose levels met the 2024 IGT diagnostic criteria published by the American Diabetes Association (ADA)⁶². Finally, unsuccessful and dead rats were excluded, and six rats that successfully modeled were selected as the IGT group for subsequent experiments. Figure 10 illustrates the experimental process.

After successful modeling, the Ctrl group ($n=6$) and the IGT group ($n=6$) continued to be fed with an ordinary diet and a high-fat diet, respectively. Blood glucose levels were measured and re-recorded on the 42nd day after a 12-hour fasting period. Subsequently, anesthesia was induced by intraperitoneal injection of a 1% sodium pentobarbital solution at a dose of 0.5 ml/100 g. After confirming deep anesthesia, blood samples were collected from the abdominal aorta via laparotomy for serum separation. Then, liver tissues were harvested on ice, frozen in liquid nitrogen immediately, and stored at -80°C in the refrigerator for long-term preservation until follow-up experiments. Euthanasia was ultimately completed by exsanguination under sustained anesthesia. This procedure was performed in accordance with the AVMA Guidelines for the Euthanasia of Animals (2020 Edition).

Main reagents

High-fat feed (67% ordinary maintenance feed + 10% oil + 20% sucrose + 2.5% sodium cholate + 0.5% cholesterol) was provided by Keao Xieyi Feed Co., LTD. (Beijing, China). Normal saline was provided by North China Pharmaceutical (Shijiazhuang, Hebei, China). Sodium citrate buffer (0.1 mol/L, pH4.5) was purchased from

Ctrl: Ordinary diet
The rest : High-fat diet

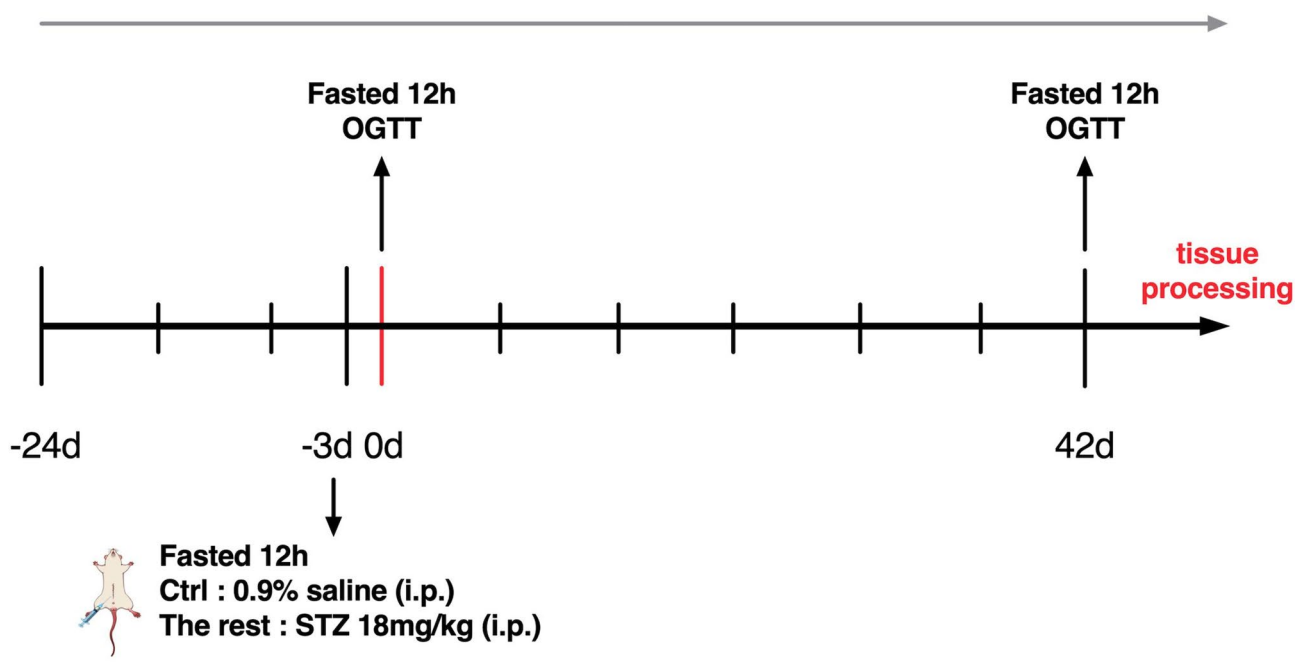


Fig. 10. Schematic representation of the experimental design. OGTT: blood glucose measurement by tail vein puncture at 30 min, 60 min, 90 min, and 120 min after gavage with 50% glucose solution. *i.p.*: intraperitoneal injection. *Ctrl*: the six rats were used for *Ctrl* group establishment. *The rest*: the rest of the 14 rats were used for the IGT model establishment.

Solarbio Technology Co., LTD. (Beijing, China). QIAzol Lysis Reagent was purchased from Qiagen (Germany). RNA Purification Kit was provided by Majorbio Bio-Pharm Technology Co. Ltd. (Shanghai, China). Biowest Agarose was purchased from Biowest (Spain). Illumina Stranded mRNA Prep, Ligation, and NovaSeq Reagent Kit were provided by Illumina (San Diego, USA).

Main instruments

TL-48R pulverizer from Wonbio Biotechnology Co., LTD. (Shanghai, China). ABSON MiFly-6 Small centrifuge from ABSON Scientific Instruments Co., LTD. (Hefei, China). Eppendorf 5424R High-speed tabletop refrigerated centrifuge from Eppendorf (Germany). DYY-6 C electrophoresis apparatus from Liuyi Biotechnology Co., LTD. (Beijing, China). NanoDrop2000 Ultramicro spectrophotometer and Qubit 4.0 Fluorescence quantifier from Thermo Fisher Scientific (Waltham, Massachusetts, USA). Agilent 5300 Bioanalyzer from Agilent (Santa Clara, California, USA). T100 Thermal Cycler PCR instrument from BIO-RAD (Hercules, California, USA). NovaSeq 6000 sequencer from Illumina (San Diego, USA).

Transcriptome sequencing

Transcriptome sequencing was performed at Shanghai Majorbio Bio-pharm Biotechnology Co., Ltd. (Shanghai, China). An appropriate amount of liver tissues was taken as samples, and total RNA was extracted according to the manufacturer's instructions for the QIAzol lysis reagent. The concentration, purity, integrity, and quality of RNA were assessed by Nanodrop2000, agarose gel electrophoresis, and Agilent 5300, respectively. High-quality RNA ($OD_{260}/280 = 1.8 \sim 2.2$, $OD_{260}/230 \geq 2.0$, $RIN \geq 6.5$, 28 S: 18 S ≥ 1.0 , $> 1 \mu\text{g}$) was selected according to the standard for the library construct.

Sequencing library construction was performed by Illumina® Stranded mRNA Prep and Ligation according to the manufacturer's instructions (Illumina, San Diego, CA). The enriched mRNA was randomly broken into 300 bp fragments, and cDNA was synthesized using reverse transcriptase and ligated to an adaptor. After further purification and selection, PCR amplification was carried out to obtain the final library. Finally, the paired-end RNA-seq library was sequenced on an Illumina NovaSeq 6000.

Differentially expressed genes and clustering analysis

Gene expression data were uploaded to the Megabio bioinformatics cloud platform. DEGs between the IGT and *Ctrl* groups were identified using DESeq2 (1.24.0) software⁶³. $P\text{adj} < 0.05$ and $\text{foldchange} \geq 2$ or ≤ 0.5 ($|\log_2\text{FC}| \geq 2$) were set as the screening threshold to obtain the initial DEGs list. Gene Ontology database (GO database, Version 2022.0915) and the Kyoto Encyclopedia of Gene and Genomes database (KEGG database, Version

2022.10) were used to perform GO enrichment and KEGG enrichment of the up- and down-regulated terms in DEGs, in order to identify the functional and metabolic pathways that DEGs were heavily and significantly enriched. A visual analysis diagram was constructed to show the direction and degree of association between different nodes, allowing for a more comprehensive understanding of the properties of DEGs and gene products, discovering upstream and downstream signaling pathways, and searching core pathways.

Western blot analysis

Our team performed Western blot analysis according to the manufacturer's instructions using the protein expression assay kit (PPAR Gamma Polyclonal antibody, NF- κ B p65 Polyclonal antibody, STAT1 Monoclonal antibody was purchased from Proteintech (IL, USA). Phospho-Stat1 (Tyr701) (D4A7) Rabbit mAb was provided by Cell Signaling Technology (Boston, USA). Anti-GAPDH, goat anti-rabbit IgG, and goat anti-mouse IgG were purchased from KeyGEN (Jiangsu, China)). The liver tissues were homogenized using a handheld homogenizer and mixed with tissue lysis buffer. After preparation, the samples were heated in sample buffer at 100°C for 5 min, and the proteins were separated by SDS-PAGE. Subsequently, proteins were transferred from the gel to a membrane and sealed with a locking buffer. The membrane was incubated overnight at 4°C with the following primary antibodies on a rocking platform: Anti-PPAR Gamma (1:1000), Anti-STAT1 (1:1000), Anti-p-STAT1 (1:1000), Anti-P65 (1:1000) and Anti-GAPDH (1:5000). The membrane was washed 3 times for 10 min each in TBST. Then, the membrane was incubated with the secondary antibody (goat anti-rabbit IgG (1:10,000) or goat anti-mouse IgG (1:10,000)) on the rocking platform and washed 3 times for 10 min each in TBST. Following this, the membrane was exposed to chemiluminescent-HRP substrate and GAPDH was used as an internal control. Finally, imaging was performed using the ChemiDoc MP Imaging System, and band gray analysis was conducted by using Gel-Pro32 software.

ELISA analysis

Forty-two days after successful modeling, whole blood collected from the abdominal aorta of the rats was placed at room temperature for 1 h and then centrifuged (1300 g) for 10 min. The supernatant serum was taken as the sample. We used the Enzyme Linked-Immuno-Sorbent Assay kit (Rat IL-6 ELISA test kit was purchased from MultiSciences (Hangzhou, China). Rat TNF-alpha ELISA Kit, Rat IL-1 beta ELISA Kit, Rat IFN-gamma ELISA Kit was purchased from Proteintech (IL, USA)) to detect and quantify serum levels of endogenous IL-6, TNF α , IL-1 β , and IFN γ . All operations were performed in strict accordance with the instructions.

Statistical analysis

In this analysis, statistical analysis of experimental data and image generation were performed by SPSS Statistics 26.0 and GraphPad Prism 10.1.2. All data are expressed as mean \pm standard deviation (SD). For comparisons between two groups, the two-tailed t-test for independent samples was used for data with a normal distribution and homogeneity of variance, and the Mann-Whitney U test was used for the data with non-normal distribution or heterogeneity of variance. $P < 0.05$ was considered statistically significant in all tests.

Data availability

The raw data has been uploaded into the Sequence Read Archive (SRA), which is hosted by the National Center for Biotechnology Information (NCBI) under the primary accession link: <https://www.ncbi.nlm.nih.gov/sra/PJRJNA1216942>.

Received: 27 January 2025; Accepted: 13 November 2025

Published online: 29 December 2025

References

1. Global, regional, and national burden of diabetes from 1990 to 2021, with projections of prevalence to 2050: a systematic analysis for the global burden of disease study 2021. *Lancet* **402**, 203–234. [https://doi.org/10.1016/s0140-6736\(23\)01301-6](https://doi.org/10.1016/s0140-6736(23)01301-6) (2023).
2. Rooney, M. R. et al. Global prevalence of prediabetes. *Diabetes Care*, **46**, 1388–1394. <https://doi.org/10.2337/dc22-2376> (2023).
3. Richter, B., Hemmingsen, B., Metzendorf, M. I. & Takwoingi, Y. Development of type 2 diabetes mellitus in people with intermediate hyperglycaemia. *Cochrane Database Syst. Rev.* **10**, Cd012661. <https://doi.org/10.1002/14651858.CD012661.pub2> (2018).
4. Li, Y. Y. et al. Analysis of influencing factors and interaction of body weight and disease outcome in patients with prediabetes. *World J. Diabetes*, **14**, 1551–1561. <https://doi.org/10.4239/wjd.v14.110.1551> (2023).
5. Luc, K., Schramm-Luc, A., Guzik, T. J. & Mikolajczyk, T. P. Oxidative stress and inflammatory markers in prediabetes and diabetes. *J. Physiol. Pharmacol.* **70** <https://doi.org/10.26402/jpp.2019.6.01> (2019).
6. Tabák, A. G., Herder, C., Rathmann, W., Brunner, E. J. & Kivimäki, M. Prediabetes: a high-risk state for diabetes development. *Lancet* **379**, 2279–2290. [https://doi.org/10.1016/s0140-6736\(12\)60283-9](https://doi.org/10.1016/s0140-6736(12)60283-9) (2012).
7. Knowler, W. C. et al. Reduction in the incidence of type 2 diabetes with lifestyle intervention or metformin. *N Engl. J. Med.* **346**, 393–403. <https://doi.org/10.1056/NEJMoa012512> (2002).
8. Zhang, P. et al. Screening and functional studies of long noncoding RNA in subjects with prediabetes. *Endocrine* **68**, 296–305. <https://doi.org/10.1007/s12020-020-02226-3> (2020).
9. Moore, C. M. & Seibold, M. A. Possibilities and promise: leveraging advances in transcriptomics for clinical decision making in allergic diseases. *J. Allergy Clin. Immunol.* **150**, 756–765. <https://doi.org/10.1016/j.jaci.2022.08.016> (2022).
10. Che, X. et al. Differently expressed genes (DEGs) relevant to type 2 diabetes mellitus identification and pathway analysis via integrated bioinformatics analysis. *Med. Sci. Monit.* **25**, 9237–9244. <https://doi.org/10.12659/msm.918407> (2019).
11. Zhao, J. et al. Bioinformatics prediction and experimental verification of key biomarkers for diabetic kidney disease based on transcriptome sequencing in mice. *PeerJ* **10**, e13932. <https://doi.org/10.7717/peerj.13932> (2022).
12. Savage, D. B., Petersen, K. F. & Shulman, G. I. Disordered lipid metabolism and the pathogenesis of insulin resistance. *Physiol. Rev.* **87**, 507–520. <https://doi.org/10.1152/physrev.00024.2006> (2007).
13. Kanehisa, M. & Goto, S. KEGG: Kyoto encyclopedia of genes and genomes. *Nucleic Acids Res.* **28**, 27–30. <https://doi.org/10.1093/nar/28.1.27> (2000).

14. Kanehisa, M., Sato, Y., Kawashima, M., Furumichi, M. & Tanabe, M. KEGG as a reference resource for gene and protein annotation. *Nucleic Acids Res.* **44**, D457–462. <https://doi.org/10.1093/nar/gkv1070> (2016).
15. Waite, K. J., Floyd, Z. E., Arbour-Reily, P. & Stephens, J. M. Interferon-gamma-induced regulation of peroxisome proliferator-activated receptor gamma and stats in adipocytes. *J. Biol. Chem.* **276**, 7062–7068. <https://doi.org/10.1074/jbc.M007894200> (2001).
16. Zhou, H. F. et al. Quercetin serves as the major component of Xiang-lian pill to ameliorate ulcerative colitis via tipping the balance of STAT1/PPAR γ and dictating the alternative activation of macrophage. *J. Ethnopharmacol.* **313**, 116557. <https://doi.org/10.1016/j.jep.2023.116557> (2023).
17. Antony, A. et al. Deficiency of Stat1 in CD11c(+) cells alters adipose tissue inflammation and improves metabolic dysfunctions in mice fed a high-fat diet. *Diabetes* **70**, 720–732. <https://doi.org/10.2337/db20-0634> (2021).
18. Tian, Y. et al. Procyanidin B2 activates PPAR γ to induce M2 polarization in mouse macrophages. *Front. Immunol.* **10**, 1895. <https://doi.org/10.3389/fimmu.2019.01895> (2019).
19. Neves, J. S. et al. Management of dyslipidemia and atherosclerotic cardiovascular risk in prediabetes. *Diabetes Res. Clin. Pract.* **190**, 109980. <https://doi.org/10.1016/j.diabres.2022.109980> (2022).
20. La Sala, L. & Pontiroli, A. E. Prevention of diabetes and cardiovascular disease in obesity. *Int. J. Mol. Sci.* **21** <https://doi.org/10.3390/ijms21218178> (2020).
21. Li, Y. et al. Peroxisome proliferator-activated receptors: A key link between lipid metabolism and cancer progression. *Clin. Nutr.* **43**, 332–345. <https://doi.org/10.1016/j.clnu.2023.12.005> (2024).
22. Mirza, A. Z., Althagafi, I. I. & Shamshad, H. Role of PPAR receptor in different diseases and their ligands: physiological importance and clinical implications. *Eur. J. Med. Chem.* **166**, 502–513. <https://doi.org/10.1016/j.ejmech.2019.01.067> (2019).
23. Guilherme, A., Virbasius, J. V., Puri, V. & Czech, M. P. Adipocyte dysfunctions linking obesity to insulin resistance and type 2 diabetes. *Nat. Rev. Mol. Cell. Biol.* **9**, 367–377. <https://doi.org/10.1038/nrm2391> (2008).
24. Labrecque, J. et al. Interleukin-1 β and prostaglandin-synthesizing enzymes as modulators of human omental and subcutaneous adipose tissue function. *Prostaglandins Leukot. Essent. Fat. Acids.* **141**, 9–16. <https://doi.org/10.1016/j.plefa.2018.11.015> (2019).
25. Farrim, M. I., Gomes, A., Milenkovic, D. & Menezes, R. Gene expression analysis reveals diabetes-related gene signatures. *Hum. Genomics.* **18**, 16. <https://doi.org/10.1186/s40246-024-00582-z> (2024).
26. McGillicuddy, F. C. et al. Interferon gamma attenuates insulin signaling, lipid storage, and differentiation in human adipocytes via activation of the JAK/STAT pathway. *J. Biol. Chem.* **284**, 31936–31944. <https://doi.org/10.1074/jbc.M109.061655> (2009).
27. Richard, A. J. & Stephens, J. M. The role of JAK-STAT signaling in adipose tissue function. *Biochim. Biophys. Acta.* **1842**, 431–439. <https://doi.org/10.1016/j.bbadi.2013.05.030> (2014).
28. Laforest, S., Labrecque, J., Michaud, A., Cianflone, K. & Tchernof, A. Adipocyte size as a determinant of metabolic disease and adipose tissue dysfunction. *Crit. Rev. Clin. Lab. Sci.* **52**, 301–313. <https://doi.org/10.3109/10408363.2015.1041582> (2015).
29. Christofides, A., Konstantinidou, E., Jani, C. & Boussiotis, V. A. The role of peroxisome proliferator-activated receptors (PPAR) in immune responses. *Metabolism* **114**, 154338. <https://doi.org/10.1016/j.metabol.2020.154338> (2021).
30. Bailey, T., Nieto, A. & McDonald, P. Inhibition of the monocarboxylate transporter 1 (MCT1) promotes 3T3-L1 adipocyte proliferation and enhances insulin sensitivity. *Int. J. Mol. Sci.* **23** <https://doi.org/10.3390/ijms23031901> (2022).
31. Jing, Y. et al. Knockout and restoration reveal differential functional roles of PPAR γ 1 and PPAR γ 2 in chicken adipogenesis. *J. Agric. Food Chem.* **70**, 14959–14973. <https://doi.org/10.1021/acs.jafc.2c05549> (2022).
32. Aprile, M. et al. PPAR γ Δ5, a naturally occurring dominant-negative splice isoform, impairs PPAR γ function and adipocyte differentiation. *Cell. Rep.* **25**, 1577–1592.e1576. <https://doi.org/10.1016/j.celrep.2018.10.035> (2018).
33. Wang, X. et al. A cross-sectional study on the associations of insulin resistance with sex hormone, abnormal lipid metabolism in T2DM and IGT patients. *Med. (Baltim.)* **96**, e7378. <https://doi.org/10.1097/md.00000000000007378> (2017).
34. Olefsky, J. M. & Glass, C. K. Macrophages, inflammation, and insulin resistance. *Annu. Rev. Physiol.* **72**, 219–246. <https://doi.org/10.1146/annurev-physiol-021909-135846> (2010).
35. Qiu, J., Shu, C., Li, X. & Zhang, W. C. PAQR3 depletion accelerates diabetic wound healing by promoting angiogenesis through inhibiting STUB1-mediated PPAR γ degradation. *Lab. Invest.* **102**, 1121–1131. <https://doi.org/10.1038/s41374-022-00786-8> (2022).
36. Zhuge, F. et al. DPP-4 Inhibition by linagliptin attenuates obesity-related inflammation and insulin resistance by regulating M1/M2 macrophage polarization. *Diabetes* **65**, 2966–2979. <https://doi.org/10.2337/db16-0317> (2016).
37. Lawrence, T. & Natoli, G. Transcriptional regulation of macrophage polarization: enabling diversity with identity. *Nat. Rev. Immunol.* **11**, 750–761. <https://doi.org/10.1038/ni3088> (2011).
38. Li, H. et al. Macrophages, chronic inflammation, and insulin resistance. *Cells* **11** <https://doi.org/10.3390/cells11193001> (2022).
39. He, L. et al. Global characterization of macrophage polarization mechanisms and identification of M2-type polarization inhibitors. *Cell. Rep.* **37**, 109955. <https://doi.org/10.1016/j.celrep.2021.109955> (2021).
40. Oh, D. Y., Morinaga, H., Talukdar, S., Bae, E. J. & Olefsky, J. M. Increased macrophage migration into adipose tissue in obese mice. *Diabetes* **61**, 346–354. <https://doi.org/10.2337/db11-0860> (2012).
41. Stafeev, Y. S. et al. Modulation of the inflammatory status of macrophages and their paracrine effect on the sensitivity of adipocytes to insulin with sirtuin and PPAR γ receptor activators. *Bull. Exp. Biol. Med.* **165**, 429–433. <https://doi.org/10.1007/s10517-018-4186-7> (2018).
42. Colao, A. et al. Relationships between serum IGF1 levels, blood pressure, and glucose tolerance: an observational, exploratory study in 404 subjects. *Eur. J. Endocrinol.* **159**, 389–397. <https://doi.org/10.1530/eje-08-0201> (2008).
43. Homan, E. P. et al. Differential roles of FOXO transcription factors on insulin action in brown and white adipose tissue. *J. Clin. Invest.* **131** <https://doi.org/10.1172/jci143328> (2021).
44. Chang, H. R., Kim, H. J., Xu, X. & Ferrante, A. W. Jr. Macrophage and adipocyte IGF1 maintain adipose tissue homeostasis during metabolic stresses. *Obes. (Silver Spring)* **24**, 172–183. <https://doi.org/10.1002/oby.21354> (2016).
45. Lv, O., Wang, L., Li, J., Ma, Q. & Zhao, W. Effects of pomegranate peel polyphenols on lipid accumulation and cholesterol metabolic transformation in L-02 human hepatic cells via the PPAR γ -ABCA1/CYP7A1 pathway. *Food Funct.* **7**, 4976–4983. <https://doi.org/10.1039/c6fo01261b> (2016).
46. Qi, Y. et al. Bile acid signaling in lipid metabolism: metabolomic and lipidomic analysis of lipid and bile acid markers linked to anti-obesity and anti-diabetes in mice. *Biochim. Biophys. Acta.* **1851**, 19–29. <https://doi.org/10.1016/j.bbalip.2014.04.008> (2015).
47. Zhang, Y. et al. Activation of the nuclear receptor FXR improves hyperglycemia and hyperlipidemia in diabetic mice. *Proc. Natl. Acad. Sci. U.S.A.* **103**, 1006–1011. <https://doi.org/10.1073/pnas.0506982103> (2006).
48. D'Esposito, V. et al. In severe obesity, subcutaneous adipose tissue cell-derived cytokines are early markers of impaired glucose tolerance and are modulated by quercetin. *Int. J. Obes. (Lond.)* **45**, 1811–1820. <https://doi.org/10.1038/s41366-021-00850-1> (2021).
49. Cheng, X., Liu, Y., Lin, N., Deng, S. & Wan, Q. Association between Interleukin-1 β polymorphism at Rs16944 and glucose metabolism: A cohort study. *Immunol. Invest.* **51**, 619–629. <https://doi.org/10.1080/08820139.2020.1860085> (2022).
50. Zhu, L., Zhao, Q., Yang, T., Ding, W. & Zhao, Y. Cellular metabolism and macrophage functional polarization. *Int. Rev. Immunol.* **34**, 82–100. <https://doi.org/10.3109/08830185.2014.969421> (2015).
51. Cho, M. J. et al. MHY2013 modulates age-related inflammation and insulin resistance by suppressing the Akt/FOXO1/IL-1 β axis and MAPK-mediated NF- κ B signaling in aged rat liver. *Appl. Immunohistochem. Mol. Morphol.* **28**, 579–592. <https://doi.org/10.1097/pai.0000000000000782> (2020).
52. Silveira, L. S. et al. Macrophage immunophenotype but not anti-inflammatory profile is modulated by peroxisome proliferator-activated receptor gamma (PPAR γ) in exercised obese mice. *Exerc. Immunol. Rev.* **26**, 10–22 (2020).

53. Mao, H., Han, B., Li, H., Tao, Y. & Wu, W. FABP4 knockdown suppresses inflammation, apoptosis and extracellular matrix degradation in IL-1 β -induced chondrocytes by activating PPAR γ to regulate the NF- κ B signaling pathway. *Mol. Med. Rep.* **24** <https://doi.org/10.3892/mmr.2021.12495> (2021).
54. Chávez-Talavera, O., Tailleux, A., Lefebvre, P. & Staels, B. Bile acid control of metabolism and inflammation in obesity, type 2 diabetes, dyslipidemia, and nonalcoholic fatty liver disease. *Gastroenterology* **152**, 1679–1694.e1673. <https://doi.org/10.1053/j.gast.ro.2017.01.055> (2017).
55. Bing, C. Is interleukin-1 β a culprit in macrophage-adipocyte crosstalk in obesity? *Adipocyte* **4**, 149–152. <https://doi.org/10.4161/21623945.2014.979661> (2015).
56. Shen, Z. et al. Expansion of macrophage and liver sinusoidal endothelial cell subpopulations during non-alcoholic steatohepatitis progression. *iScience* **26**, 106572. <https://doi.org/10.1016/j.isci.2023.106572> (2023).
57. Thomas, A. P., Dunn, T. N., Oort, P. J., Grino, M. & Adams, S. H. Inflammatory phenotyping identifies CD11d as a gene markedly induced in white adipose tissue in obese rodents and women. *J. Nutr.* **141**, 1172–1180. <https://doi.org/10.3945/jn.110.127068> (2011).
58. Zhai, M. et al. Identification of three significant genes associated with immune cells infiltration in dysfunctional adipose tissue-induced insulin-resistance of obese patients via comprehensive bioinformatics analysis. *Int. J. Endocrinol.* **2021**, 8820089. <https://doi.org/10.1155/2021/8820089> (2021).
59. Li, B., Zhao, X., Xie, W., Hong, Z. & Zhang, Y. Integrative analyses of biomarkers and pathways for diabetic nephropathy. *Front. Genet.* **14**, 1128136. <https://doi.org/10.3389/fgene.2023.1128136> (2023).
60. Krishnamurti, D. G. B., Purwaningsih, E. H., Tarigan, T. J. E., Soetikno, V. & Louisa, M. Hematological indices and their correlation with glucose control parameters in a prediabetic rat model. *Vet. World* **15**, 672–678. <https://doi.org/10.14202/vetworld.2022.672-678> (2022).
61. Hoffman, E. G. et al. Effects of somatostatin receptor type 2 antagonism during insulin-induced hypoglycaemia in male rats with prediabetes. *Diabetes Obes. Metab.* **25**, 1547–1556. <https://doi.org/10.1111/dom.15002> (2023).
62. Introduction and Methodology. Standards of care in diabetes-2024. *Diabetes Care* **47**, S1–s4. <https://doi.org/10.2337/dc24-SINT> (2024).
63. Love, M. I., Huber, W. & Anders, S. Moderated estimation of fold change and dispersion for RNA-seq data with DESeq2. *Genome Biol.* **15**, 550. <https://doi.org/10.1186/s13059-014-0550-8> (2014).

Acknowledgements

The authors are grateful to Professor Chunguo Wang from the Beijing University of Chinese Medicine for assistance in the data analysis. The authors thank AiMi Academic Services (www.aimieditor.com) for English language editing and review services. The data of transcriptomic were analyzed through the free online platform of majorbio cloud platform (cloud.majorbio.com).

Author contributions

R.Y. wrote the draft of the manuscript and participated in the animal exercise experiments. Y.X. wrote the draft of the manuscript and designed the experiments. Y.F. and X.L. participated in the animal exercise experiments. Z.Y. analyzed the data. S.L. edited and revised the manuscript. All authors reviewed the manuscript and approved the submitted version.

Declarations

Competing interests

The authors declare no competing interests.

Additional information

Supplementary Information The online version contains supplementary material available at <https://doi.org/10.1038/s41598-025-28985-5>.

Correspondence and requests for materials should be addressed to S.L.

Reprints and permissions information is available at www.nature.com/reprints.

Publisher's note Springer Nature remains neutral with regard to jurisdictional claims in published maps and institutional affiliations.

Open Access This article is licensed under a Creative Commons Attribution-NonCommercial-NoDerivatives 4.0 International License, which permits any non-commercial use, sharing, distribution and reproduction in any medium or format, as long as you give appropriate credit to the original author(s) and the source, provide a link to the Creative Commons licence, and indicate if you modified the licensed material. You do not have permission under this licence to share adapted material derived from this article or parts of it. The images or other third party material in this article are included in the article's Creative Commons licence, unless indicated otherwise in a credit line to the material. If material is not included in the article's Creative Commons licence and your intended use is not permitted by statutory regulation or exceeds the permitted use, you will need to obtain permission directly from the copyright holder. To view a copy of this licence, visit <http://creativecommons.org/licenses/by-nc-nd/4.0/>.

© The Author(s) 2025